Structural Similarity of Turbulence in Fully Developed Smooth Pipe Flow

J. C. S. Lai*
University of New South Wales, Canberra, Australia
K. J. Bullock†
University of Queensland, St. Lucia, Australia
and
R. E. Kronauer‡
Harvard University, Cambridge, Massachusetts

The structure of fully developed turbulence in a smooth pipe has been studied in detail for a Reynolds number of 134,000 (based on centerline velocity and pipe radius) at two fixed distances from the wall, namely, $y^+ = 70$ and 200. Correlations of the longitudinal component of turbulence were generated simultaneously in seven narrow-frequency bands using an automated data acquisition system that jointly varied the longitudinal and transverse separations of two hot-wire probes. By taking Fourier transforms of the correlations, power spectral density functions were obtained with frequency ω and longitudinal and transverse wave numbers k_x and k_z as independent variables. The data presented in this form show the distribution of turbulence intensity among waves of different size and inclination, providing an estimate of the convection velocity of individual waves. A wave size range of about 20 has been covered by the data. With appropriate analysis and interpretation, the convection velocity results fully support the similarity hypothesis.

Nomenclature

A	= wave strength function
C_x	= streamwise phase velocity
C_z	= circumferential phase velocity
f	= wave intensity function
k	= resultant wave number $= [k_x^2 + k_z^2]^{1/2}$
k_x, k_z	= longitudinal (x) and transverse (z) wave numbers, respectively
$P(k_x^+, k_z^+, \omega^+)$	= power spectral density function
R	= radius of pipe
$R_{ij}(\Delta x^+, \Delta z^+, \tau)$	= correlation function
$R_{ij}(\Delta x^+, \Delta z^+ \mid \omega^+)$	= filtered correlation function
t	= time
U	= mean velocity in the x direction
u, v, w	= turbulent velocities in the Cartesian x, y, and z directions, respectively
$\hat{u}, v, \hat{w}$	= turbulent velocities in the wave coordinate $\hat{x}$, y, and $\hat{z}$ directions, respectively
u_τ	= friction velocity
y_0	= distance of measurement station from the pipe wall
α	= wave angle
Δ	= difference between two quantities
ν	= kinematic viscosity
τ	= time delay
ω	= circular frequency (rad/s)

Superscripts

+	= quantity nondimensionalized using u_τ and ν
$(^-)$	= time average

I. Introduction

WITH the advent of conditional sampling and computing techniques, the structure of turbulence has been extensively investigated in the past two decades to provide some understanding of its mechanism and, hence, to predict and improve the performance of heat and momentum transfer in everyday engineering situations. Fully developed flow in a smooth pipe constitutes one of the simplest cases of shear flow turbulence and is the subject of this paper. Following the visualization studies[1-4] of low Reynolds number flows and numerous velocity correlation and spectra measurements[5,6] at higher Reynolds numbers, the traditional classification of fully developed pipe flow into three distinct regions based on measurements of the mean velocity profile, namely, the viscous sublayer, a buffer layer, and the turbulent core, has been questioned and re-examined. Fage and Townend[7] were among the first to indicate that the sublayer was not truly laminar but consisted of small-scale turbulence. This was later supported by the hot-wire measurements of Laufer[5] and the flow visualization work of Corino and Brodkey.[3] For relatively low Reynolds number between 10,600 and 46,400, Morrison et al.[8] concluded from their two-dimensional spectra measurements that the sublayer turbulence is wave-like, but results just outside the sublayer suggest that, for a Reynolds number greater than 30,000, the structure will change substantially as it blends into the remaining general turbulent field. All of these results, including the narrow-band frequency radial correlation measurement of Bullock et al.,[9] imply that the boundary layer has a continuous structure instead of several distinct layers each of which displays its own characteristic behavior.

The turbulent velocity field in a smooth circular pipe can be described by two-point space-time correlations that involve three velocity components with six pair combinations. By assuming stationarity in space x,z and time t variables (defined

Received Oct. 14, 1987; revision received March 11, 1988. Copyright © American Institute of Aeronautics and Astronautics, Inc., 1988. All rights reserved.

*Senior Lecturer, Department of Mechanical Engineering, University College. Member AIAA.
†Professor, Department of Mechanical Engineering.
‡Professor, Division of Engineering and Applied Physics.

in Fig. 1), there are still five arguments in the correlation functions: $x_1 - x_2$, $z_1 - z_2$, $t_1 - t_2$, y_1, and y_2. A description of turbulence by multipoint space-time correlations would render the interpretation of these data almost impossible. Morrison and Kronauer[10] successfully demonstrated that turbulence can be interpreted by a stochastic wave model with coordinates as specified in the wave schematic diagram in Fig. 2. The measurable velocity fluctuations in the x and z directions are given by

$$u = \hat{u}\cos\alpha + \hat{w}\sin\alpha \tag{1a}$$

$$w = \hat{w}\cos\alpha - \hat{u}\sin\alpha \tag{1b}$$

By introducing a similarity variable k^+y^+ based on the wave number k^+ and the distance y^+ from the wall, Morrison and Kronauer[10] were able to collapse their turbulence data in wave number space. In particular, the change in the intensity of the two-dimensional power density function $P(\omega^+, k^+y^+)$ can be described as the product of an intensity function $f(k^+y^+)$ and the universal wave strength function A as given by

$$P(\omega^+, k^+y^+) = f(k^+y^+)\, A(\omega^+, k_z^+) \tag{2}$$

With the introduction of a correction procedure that is independent of Reynolds number and applicable to waves of all sizes, they were also able to extend the similarity concept from the region where the mean velocity profile is logarithmic down to the sublayer regions. More recent work by Perry and Abell[11] shows that the turbulence intensity correlates well through a similarity variable for the region between $y^+ = 100$ and $y/R = 0.1$. The wall-pressure fluctuation data of Bull[12] and the static pressure and velocity fluctuations data of Elliot[13] are consistent with the measurements of Morrison and Kronauer.[10] Radial correlations and spectra of longitudinal velocity fluctuations obtained by Bullock et al.[9] further supported the similarity hypothesis and the use of a stochastic wave model in interpreting turbulence data in fully developed pipe flow.

A stochastic wave model does not necessarily imply that the flow is composed physically of geometrically similar waves but is just one way of describing the mechanism of turbulence through compact reduction of data. In addition, interchange of energy between different scales of disturbances can be examined through the power density distribution functions. Such a wave model, if verified to be valid, reduces considerably the amount of data to be interpreted and can provide and extract useful information for the mechanism of turbulence. In the stochastic wave model, only the v component of the velocity fluctuation is independent of the wave angle α and can be used by itself to test the similarity hypothesis. Unfortunately, this is also the most difficult to measure close to a surface.[14]

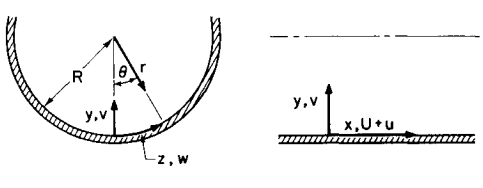

Fig. 1 Pipe coordinates and velocity components.

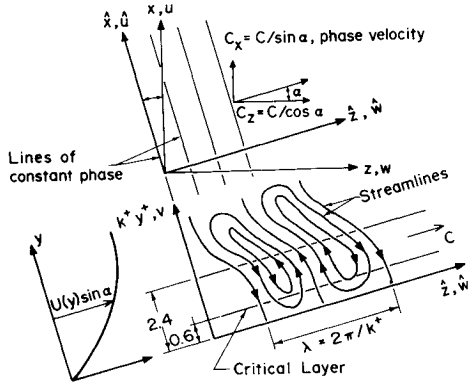

Fig. 2 Wave schematic diagram.

McConachie[15] presented the three-dimensional spectral density function $P(k_x^+, k_y^+, \omega^+)$ for a Reynolds number of 69,000 (based on centerline velocity and radius) and at a distance from the wall of $y^+ = 70$. The measurements were taken in a pipe of 133.4 mm diam with a friction velocity u_τ of 0.61 m/s. His data of wave convection velocity C_x^+ as a function of wave size k^+ for three different frequencies $\omega^+ = 0.042$, 0.0853, and 0.171 did not collapse onto a single curve unless modified by an empirical function of frequency $S(\omega^+)$. However, this inevitably contradicts the basic premise of the similarity hypothesis; that is, only relative motions are relevant, and hence absolute frequency is irrelevant.

The aims of this study were to explore further the apparent contradictions between the results of McConachie[15] and those reported in the literature (e.g., Morrison and Kronauer[10]) by obtaining new three-dimensional spectra at $y^+ = 70$ and 200, both for a friction velocity u_τ of 0.61 m/s. Furthermore, the project was designed to examine evidence of the structural similarity in turbulent pipe flow and to interpret this if possible using a wave-model concept.

II. Experimental Conditions

Results of Morrison and Kronauer[10] indicate that the waves are distributed uniformly over a range bounded at one extreme by the geometric constraint of the pipe ($k_{\min}^+ \simeq 2\pi/R^+$) and at the other extreme by the dissipative action of viscosity ($k_{\max}^+ \simeq 0.05$). A friction velocity u_τ of 0.61 m/s will, therefore, provide a wave size range of 40 and corresponds to a flow Reynolds number of 134,000 based on the pipe radius and the centerline velocity. Correlation measurements in u were taken at two positions from the pipe wall, namely, 1) $y^+ = 70$, which adequately covers the waves of small inclination as shown by McConachie,[15] and 2) $y^+ = 200$, which selects waves of longer wavelength. The measurements were taken in fully developed pipe flow in a tunnel of 254 mm diam, almost twice that used by McConachie.[15] The correlation function and the cross-power spectral density function are, of course, conjugate forms of the same data, and neither contains more information than the other. However, it is more appropriate to interpret the data in the wave number/frequency space, as is evident in the product decomposition of Eq. (2).

In this study, the Fourier transform in the time variable was bypassed by filtering the turbulent fluctuation signals from two hot wires simultaneously with seven pairs of bandpass filters, giving the filtered correlations $R_{ij}(\Delta x^+, \Delta z^+ \omega^+)$. The center frequencies of the filters used were 205, 257, 325, 409, 515, 650, and 819 Hz, corresponding to $\omega^+ = 0.0536$, 0.0672, 0.0850, 0.1070, 0.1374, 0.1700, and 0.2142, respectively. With a filter bandwidth of 7.5%, an integration period of 120 s was used, yielding results with a statistical uncertainty of 0.1% for the lowest frequency used (i.e., 205 Hz). The correlation in u was normalized so that, in terms of the nondimensional variables, it is given by

$$R_{uu}(\Delta x^+, \Delta z^+ \omega^+) = \frac{\overline{u(x^+, z^+ \omega^+)\, u(x^+ + \Delta x^+, z^+ + \Delta z^+ | \omega^+)}}{[\overline{u^2(x^+, z^+ \omega^+)}\ \overline{u^2(x^+ + \Delta x^+, z^+ + \Delta z^+ | \omega^+)}]^{1/2}} \tag{3}$$

For simplicity, hereafter $R_{uu}(\Delta x^+,\Delta z^+|\omega^+)$ is written as $R(x^+,z^+\omega^+)$. As pointed out by Morrison and Kronauer,[10] it is convenient to present spectra on logarithmic wave number scales so that the following power spectral density functions are defined:

$$P(k_x^+,k_z^+,\omega^+) = \frac{2}{\pi^2}k_x^+k_z^+\int_0^\infty\int_0^\infty R(x^+,z^+|\omega^+) \times [\cos(k_x^+x^+ + k_z^+z^+) + \cos(k_x^+x^+ - k_z^+z^+)]dx^+dz^+ \quad (4)$$

$$P(k_x^+\omega^+) = \frac{2}{\pi}k_x^+\int_0^\infty R(x^+,0|\omega^+)\cos(k_x^+x^+)\,dx^+ \quad (5)$$

$$P(k_z^+\omega^+) = \frac{2}{\pi}k_z^+\int_0^\infty R(0,z^+|\omega^+)\cos(k_z^+z^+)\,dz^+ \quad (6)$$

with integrals given by

$$\int_0^\infty P(k_x^+,k_z^+,\omega^+)\,d(\ell n\,k_x^+)\,d(\ell n\,k_z^+) = 1.0 \quad (7a)$$

$$\int_0^\infty P(k_x^+,\omega^+)\,d(\ell n\,k_x^+) = 1.0 \quad (7b)$$

$$\int_0^\infty P(k_z^+,\omega^+)\,d(\ell n\,k_z^+) = 1.0 \quad (7c)$$

For $y^+ = 70$, a total of 1306 spatial separations were used for generating the correlation $R(x^+,z^+|\omega^+)$, with a maximum longitudinal separation $x^+ = 6500$ and a maximum transverse separation $z^+ = 572.28$ (6.65 deg). The longitudinal and transverse resolutions $\Delta x^+ = 40$ and $\Delta z^+ = 30.12$ correspond, respectively, to spatial Nyquist wave numbers of $k_x^+ = 0.079$ and $k_z^+ = 0.10$. For $y^+ = 200$, the correlations $R(x^+,z^+|\omega^+)$ were generated for a total of 2551 spatial separations, with a maximum longitudinal separation $x^+ = 10{,}500$ and a maximum transverse separation $z^+ = 1382.22$ (16.5 deg). The longitudinal and transverse resolutions $\Delta x^+ = 40$ and $\Delta z^+ = 25.13$ correspond, respectively, to spatial Nyquist wave numbers of $k_x^+ = 0.079$ and $k_z^+ = 0.125$.

III. Experimental Apparatus

The smooth steel pipe of 254 mm i.d. is 14.675 m long, with a surface roughness of 63 CLA. The testing section is located downstream at stations between 52.75 and 56.75 pipe diameters and is circular within 0.1 mm and straight within 0.001 mm/mm of the axial length. Air, supplied by a shunt-wound dc electric motor, is first passed through a heat exchanger to keep its temperature constant. A wire gauze is placed at the entrance of the pipe to promote flow development. Swirl and large-scale turbulence generated by the blower and associated diffuser are eliminated by a settling chamber.

The facility allows introduction of two hot-wire anemometer probes radially into the pipe, one through a straight slot (525 mm long × 19 mm wide) along the pipe axis and the other through a right-angled slot (107 deg in extent and 19 mm wide).

The hot-wire sensors were single tungsten wires, each copper-plated at two ends with a working section of 5 μ diam and 0.5 mm length operated at a resistance ratio of 1.3. The working section of each wire and its associated image on the polished wall was measured with a Rank-Taylor alignment telescope, giving an accuracy of 12.7 μ for determining the wire separation from the wall.

The longitudinal separation of the two wires can be determined by measuring with an alignment telescope the distance between their images in a 45-deg prism placed under the wires. The prism also enables the wires to be set parallel to each other and the position of zero transverse separation to be accurately defined.

Following studies by Comte-Bellot et al.[16] on aerodynamic disturbance caused by simple hot-wire probes, the hot-wire probes were designed to minimize this effect with the probe's final section of the stem at 45 deg to the mean-flow direction, the prong's spacing about 25 prong diameters, and the prong at least six prong diameters from the working section of the wire. The working section of the wire is asymmetrical with respect to the prongs in order to enable a full traverse in the transverse direction with minimal interference from the prongs of the upstream probe (Fig. 3).

During the experiment, both the total turbulence intensity and the narrow-band turbulence intensity recorded by the two probes were monitored. For $40 < x^+ < 100$, the total turbulence intensity recorded by the two probes and the turbulence intensity in each frequency band differed by less than 20%. For $x^+ > 500$, the probe interference effect is minimal.

IV. Correlation and Spectra Results

A hot-wire traverse across the pipe at the testing section yields a velocity distribution that follows the universal log-law profile and a longitudinal turbulence intensity distribution in good agreement with the data of Laufer.[5] Figure 4 shows some of the representative correlation results $R(x^+,z^+|\omega^+)$ for four different frequencies ω^+ at $y^+ = 200$ and for $x^+ = 0$, 80, 160, 360, and 760. The results for $y^+ = 70$, in general, show a similar trend. The correlation data were transformed to give the power spectral density function $P(k_x^+,k_z^+,\omega^+)$ described by Eq. (4). It must be pointed out that, in generating the power spectra $P(k_x^+,k_z^+,\omega^+)$, regions of negative values of $P(k_x^+,k_z^+,\omega^+)$ can be identified. Negative $P(k_x^+,k_z^+,\omega^+)$ is not a physical possibility and must be due to measurement errors associated with finite length correlations, finite spatial sampling, and probe interference effects. Nevertheless, for both $y^+ = 70$ and $y^+ = 200$, the integral of $P(k_x^+,k_z^+,\omega^+)$ over the wave number (k_x^+,k_z^+) space for the various ω^+ amounts to at least 0.85, typically 0.9, compared with the expected normalized value of 1.0, as indicated in Eqs. (7).

The contours for the power spectral density function $P(k_x^+,k_z^+,\omega^+)$ obtained for various ω^+ are shown in Figs. 5 and 6, respectively, for $y^+ = 70$ and $y^+ = 200$. The results for three other frequencies $\omega^+ = 0.0672$, 0.1070, and 0.1700, although not shown here, do have similar characteristics. Al-

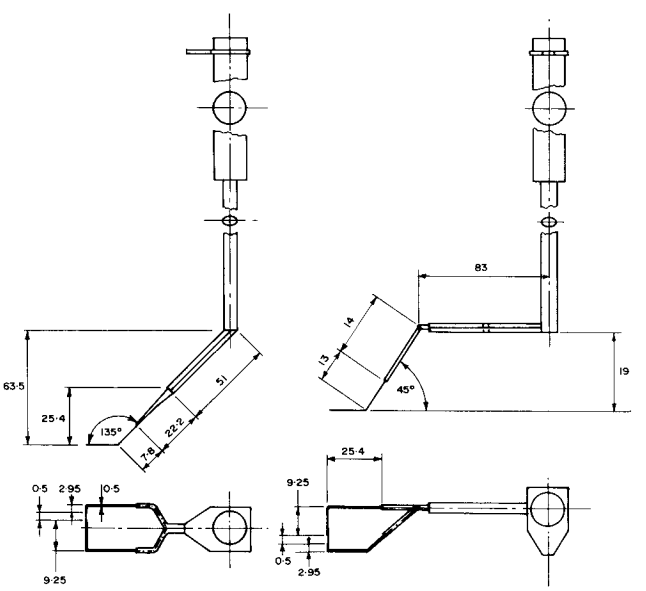

Fig. 3 Details of hot-wire probes (dimensions in mm).

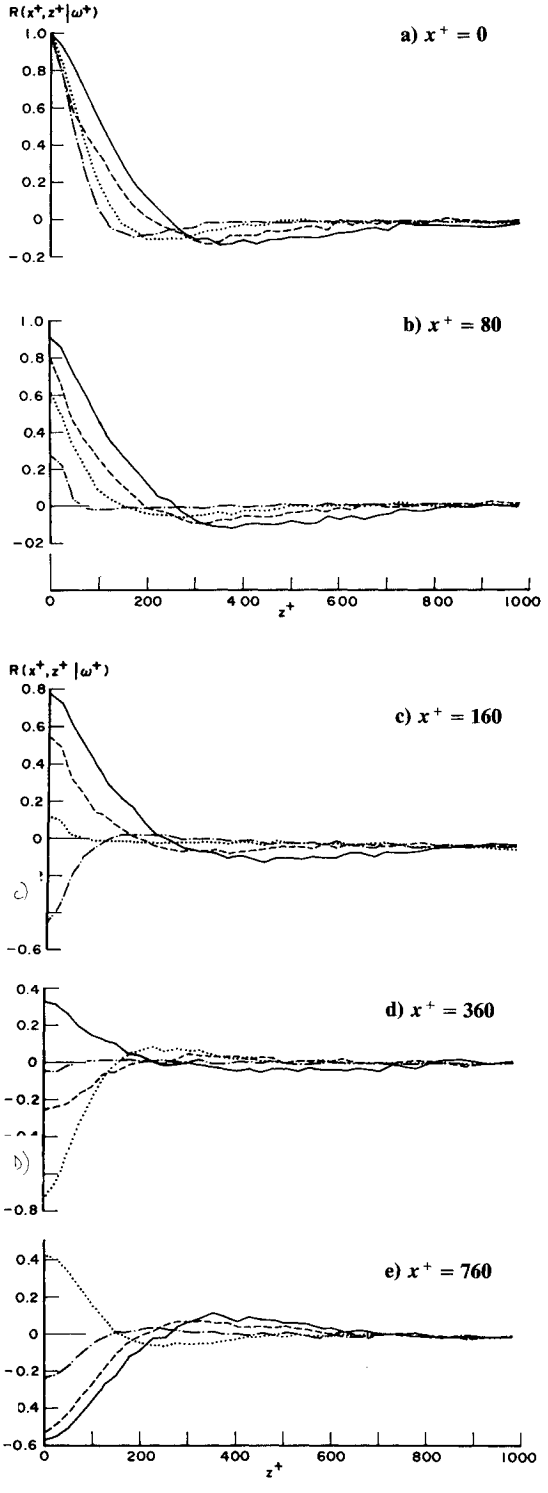

Fig. 4 Two-dimensional correlation $R(x^+,z^+,|\omega^+)$ at $y^+ = 200$ for —— $\omega^+ = 0.0536$, ---- $\omega^+ = 0.085$, ···· $\omega^+ = 0.1347$, and - · - $\omega^+ = 0.2142$.

though for $y^+ = 70$ the exact contour details differ from those reported by McConachie,[15] they do indicate similar trends and cover similar range of wave angles α.

The narrow-band frequency filters basically select waves of particular sizes in the wave number (k_x^+,k_z^+) space. In order to illustrate the general effects of frequency ω^+ and the distance from the wall y^+ on the power spectra, the spectral peaks for various ω^+ are plotted in Fig. 7. Lines of constant wave size k^+ and constant wave angle α are also indicated. The lines of best fit to the data of the spectral peaks for $y^+ = 70$ and 200 are given, respectively, by

$$k_z^+ = 0.0052 + 1.47\ k_x^+ \tag{8a}$$

with a correlation coefficient of 0.97, and

$$k_z^+ = 0.0029 + 1.16\ k_x^+ \tag{8b}$$

with a correlation coefficient of 0.99.

Figure 7 shows that, at a given distance from the wall, the spectral peak moves from a smaller wave angle at lower frequency to a larger wave angle at higher frequency. The constant k^+ arcs of Fig. 7 also represent constant phase velocity C^+. Since there is a constraint on the minimum size of k_z^+ ($= 2\pi/R^+ = 0.00126$) and no such constraint on k_x^+, as the wave size component sampled at a particular ω^+ and y^+ is increased, there are more lower α waves, that is, more $\hat{u}$ component in u (Fig. 2). For a given ω^+, the spectral peak at $y^+ = 200$ is associated with a wave of larger size and larger wave angle than at $y^+ = 70$. Furthermore, for a given ω^+, waves of the smaller size which exist at $y^+ = 70$ do not extend to $y^+ = 200$. This result is consistent with the data of Morrison and Kronauer,[10] where, for data over a y^+ range of 49 to 395 for shear velocities of 0.61 and 0.85 m/s, the shift in the spectral peak in a (ω^+,k_z^+) plot [approximately equivalent to a (k_x^+,k_z^+) graph] for increasing y^+ is always to a larger α and smaller k^+.

Within the limits of experimental error, the ratio of the spectral peak wave size at $y^+ = 200$ to that at $y^+ = 70$ may be considered to be independent of ω^+ and is given by an average value of $k^+{}_{70}/k^+{}_{200} = 0.70$. Furthermore, the spectral peak at both $y^+ = 70$ and 200 appears to convect at a constant streamwise phase velocity independent of ω^+. For $y^+ = 70$, the average streamwise phase velocity of the spectral peak is about 0.95 times that of the local mean velocity, whereas that at $y^+ = 200$ is about 0.93 times that of the local mean velocity.

V. Convection Velocity Results

As already indicated in Fig. 2, a point in (ω^+,k_x^+,k_z^+) wave space represents a wave with total wave number k^+ and with lines of constant phase inclined to the x axis (pipe axis) at the angle α when projected radially outward to the pipe surface. Such a wave exhibits a streamwise phase velocity given by

$$C_x^+ = \omega^+/k_x^+ = C_x/u_\tau \tag{9}$$

and a circumferential phase velocity (projected on the pipe surface) given by

$$C_z^+ = \omega^+/k_z^+ = C_z/u_\tau \tag{10}$$

The mean streamwise convection velocity C_x^+ is defined by the locus of the ridge line of $P(k_x^+,k_z^+,\omega^+)$ plot for each ω^+, as shown in Figs. 5 and 6. The variation of the mean streamwise convection velocity C_x^+ with wave number k^+ at $y^+ = 70$ is shown in Fig. 8a for all seven frequencies ω^+. It is immediately obvious that the C_x^+ data for various ω^+ do not collapse onto a single curve, a trend reported by McConachie,[15] thus contradicting the similarity hypothesis. However, a closer examination of the data in Fig. 8a reveals that, for the medium frequency range $\omega^+ = 0.085$ to 0.1347, they do collapse onto a single curve. Furthermore, if the geometrically similar wave model of Morrison and Kronauer[10] is assumed, then, by using the concept of critical layer (the wave speed C^+ matches the mean velocity component projected into the wave cross section at a distance y_0^+ from the wall such that $k^+y_0^+ = \beta$ is a constant), the mean streamwise convection velocity will be given by

$$C_x^+ = 2.5\ \ell n(\beta/k^+) + 5.5 \tag{11}$$

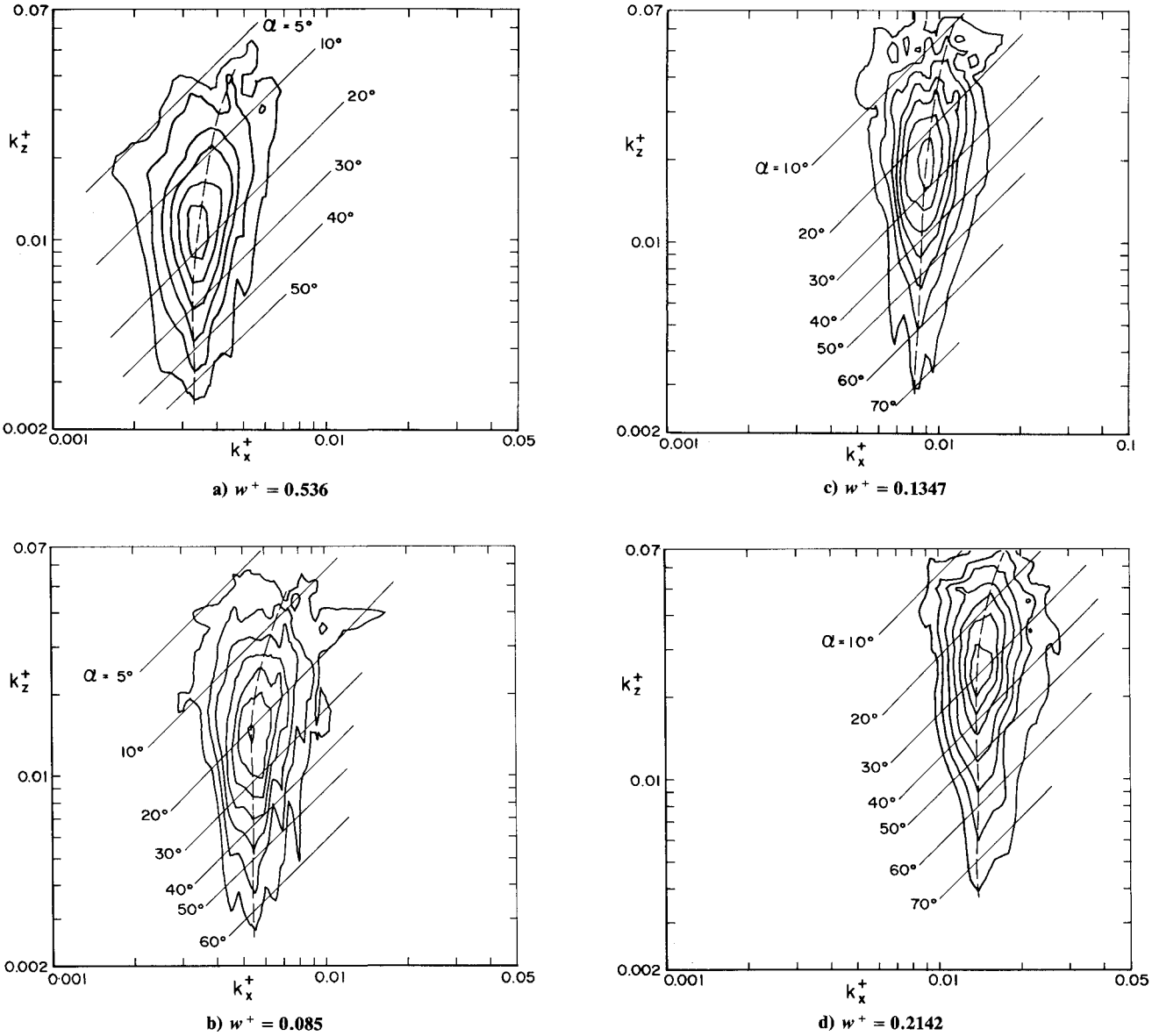

Fig. 5 Contours of power spectral density function $P(k_x^+, k_z^+, \omega^+)$ at $y^+ = 70$ (contour minimum 0.1, step 0.1).

Indeed, the line given by $\beta = 0.85$ fits the data for the medium-frequency range, as shown in Fig. 8a. That the low- and high-frequency data do not collapes onto a single curve requires careful consideration. The correlation data for the high frequencies such as $\omega^+ = 0.2142$ (not presented here but similar to those at $y^+ = 200$ in Figs. 4b–4d reveal significant probe interference effects for small separations x^+ and z^+ (that is, correlation results lower than actual), so that the power spectral density functions $P(k_x^+, k_z^+, \omega^+)$ obtained from Fourier transform will tend to be underestimated for high k_x^+, leading to a shift in the contours of high k^+ toward lower k_x^+. To illustrate the sensitivity of the convection velocity results, consider the ridge line locus for $P(k_x^+, k_z^+, \omega^+)$ and $\omega^+ = 0.2142$ at (0.0157, 0.047), which gives a $C_x^+ = 13.64$ at $k^+ = 0.0496$. A point (0.0167, 0.047) in wave number space will give a $C_x^+ = 12.83$ with $k^+ = 0.0499$, which fits the line given by $\beta = 0.85$ in Fig. 8a very well. However, the correction applied to k_x^+ is only 6%, thus indicating that the convection velocity is a very sensitive test for the correlation and spectra results. On the other hand, for the low-frequency data such as $\omega^+ = 0.0536$, it is conceivable from both the correlation data and the transformed data $P(k_x^+, k_z^+, \omega^+)$ (Fig. 5) that both the maximum longitudinal and transverse traverse is not sufficient, resulting in overestimation of k_x^+ associated with the power density spectra results at low k^+.

Nevertheless, for the medium-frequency range, the probe interference effect at small separations is not as severe as for the high frequencies, and the extent of both the longitudinal and transverse traverse may be sufficient compared with the low frequencies because the waves selected are of shorter wavelength. However, it may be seen from Fig. 8 for $k^+ < 0.01$ in the medium-frequency range that, for a given ω^+, the convection velocity data obtained at low k^+ are more affected than at high k^+ if the extent of traverse is insufficient. Hence, with sufficient traverse in both the longitudinal and transverse directions at low frequencies (which inevitably means much longer experimental time to resolve only the small correlation values at the tails) and better probe design for the hot wires to eliminate interference effects at high frequencies, the convection velocity data C_x^+ are expected to collapse onto a single curve, as is exhibited here by the medium-frequency data (Fig. 8a). It must be emphasized that probe interference

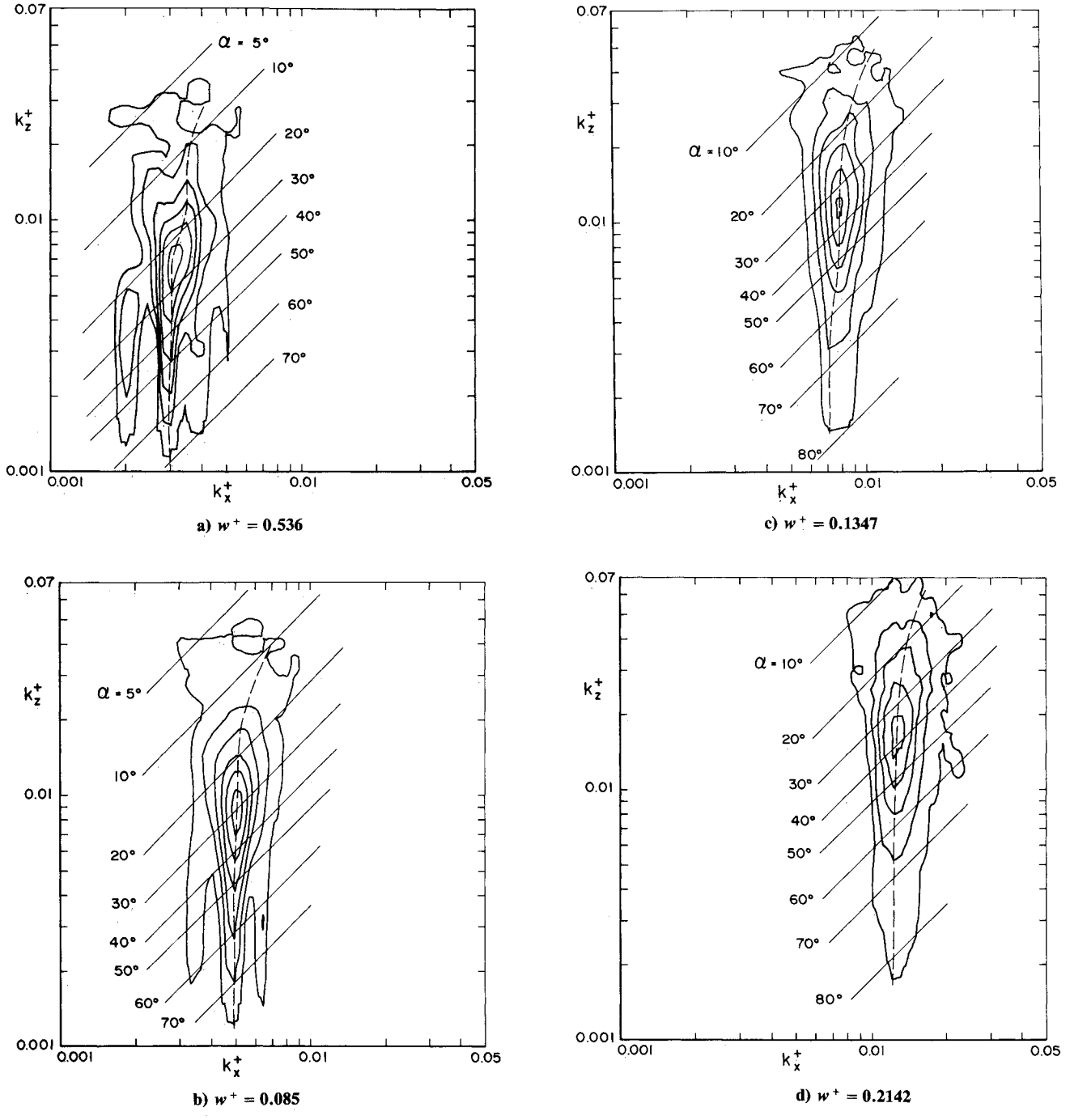

Fig. 6 Contours of power spectral density function $P(k_x^+, k_z^+, \omega^+)$ at $y^+ = 200$ (contour minimum 0.1, step 0.2).

effects are inherent in hot-wire measurements, being more severe at high frequencies and, hence, small wavelengths.

From the spectral peak plot in Fig. 7, it is expected that the extent of longitudinal and transverse traverse at $y^+ = 200$ will be even more insufficient compared with that at $y^+ = 70$ as the waves are of longer wavelength. This explains the peculiar shape of the contours for $P(k_x^+, k_z^+, \omega^+)$ at low k^+, especially for low frequencies such as $\omega^+ = 0.0536$ shown in Fig. 6a. Furthermore, the probe interference effects at high frequencies are obviously much more severe than at low frequencies, as shown in Fig. 4. Nevertheless, it is encouraging to observe that the convection velocity data C_x^+ determined from the locus of the ridge line of $P(k_x^+, k_z^+, \omega^+)$ for the medium frequency range do collapse onto a single curve described by Eq. (11) with $\beta = 1.28$, as shown in Fig. 8b. Moreover, the ratio of β at $y^+ = 70$ to β at $y^+ = 200$ is 0.664, which is very consistent with the ratio of wave sizes determined by the spectral peaks in Sec. IV, which is 0.70. Although this value is smaller than the expected logarithmic distribution that will give a ratio of $\ell n 70/\ell n\, 200 = 0.8$, it is modified by the influence of the spatial extent and probe interference effects of the correlation measurements and the dominance of $\hat{w}$ in the measurable u fluctuation [Eq. (1)] for large wave angle α at $y^+ = 200$.

VI. Structural Similarity of Turbulence

The basic principles of the similarity hypothesis are listed as follows:

1) There is only one characteristic length scale, that is, distance from the wall y (or y^+).

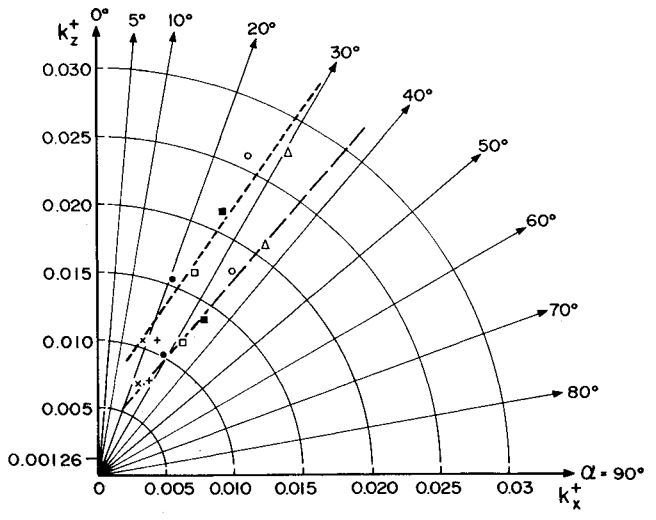

Fig. 7 Locus of spectral peaks in wave number (k_x^+, k_z^+) space: --- $y^+ = 70$, ---- $y^+ = 200$, $x\,\omega^+ = 0.0536$, $+\,\omega^+ = 0.0672$, ● $\omega^+ = 0.085$, □ $\omega^+ = 0.107$, ■ $\omega^+ = 0.1347$, ○ $\omega^+ = 0.17$, △ $\omega^+ = 0.2142$.

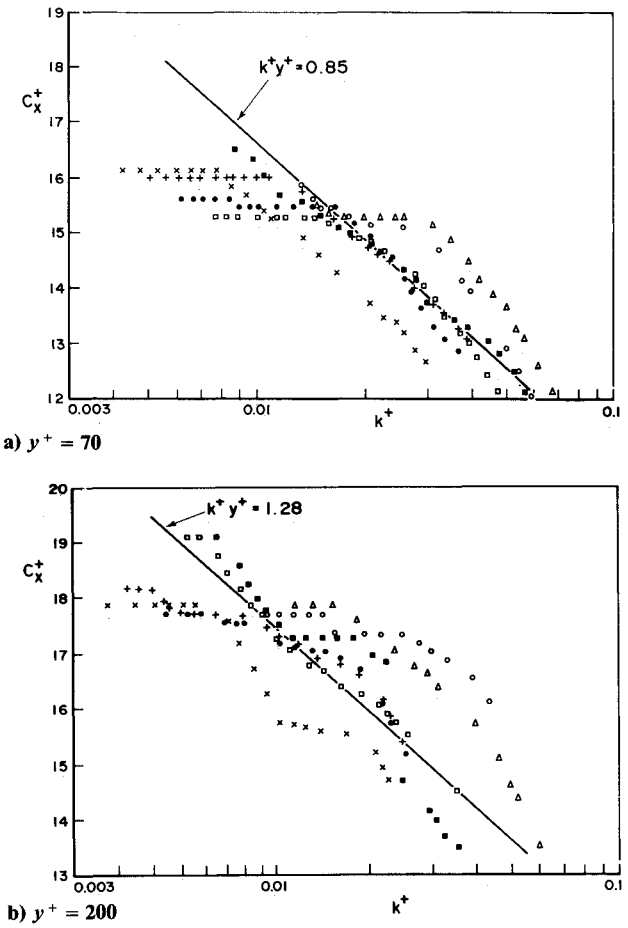

Fig. 8 Variation of mean streamwise convection velocity C_x^+ with wave number k^+ (symbols as in Fig. 7).

2) There is only one characteristic time scale, that is, $(dU^+/dy^+)^{-1}$. Because of the logarithmic distribution of the mean velocity U^+, this time scale is proportional to y^+.

3) Absolute velocity is irrelevant, and only velocity relative to the local velocity U is relevant.

As a result of principle 3, the experimental data for convection velocity, spectral sheet thickness, and spectral peaks will be examined for structural similarity in a coordinate system

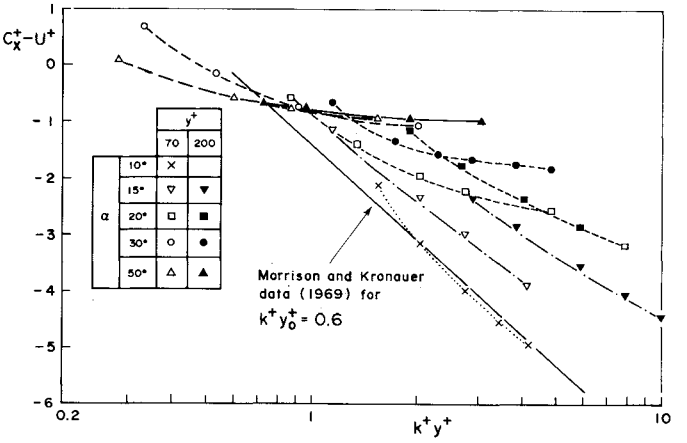

Fig. 9 Variation of $[C_x^+ - U^+(y_0^+)]$ with k^+y^+ for various α: —— Morrison and Kronauer data (1969) for $k^+y_0^+ = 0.6$. For $y^+ = 70$, × $\alpha = 10$ deg, ▽ $\alpha = 15$ deg, □ $\alpha = 20$ deg, ○ $\alpha = 30$ deg, △ $\alpha = 50$ deg. For $y^+ = 200$, ▼ $\alpha = 15$ deg ■ $\alpha = 20$ deg, ● $\alpha = 30$ deg, ▲ $\alpha = 50$ deg.

with no relative motion, that is, a coordinate system moving with the average local speed $U^+(y^+)$.

Convection Velocity Data

Consider a two-dimensional power spectrum as a function of ω^+ and k_x^+. Then, the frequency half-bandwidth $(\Delta\omega^+)^{-1}$ associated with each k_x^+ can be interpreted as the typical lifetime for a disturbance of that size, and $\Delta\omega^+$ is referred to here as the spectral sheet thickness. In a coordinate system with no relative motion, this is expressed as follows:

$$\Delta\omega^+ = \omega^+ - U^+ k_x^+ \tag{12}$$

If $(\Delta\omega^+)^{-1}$ is normalized by the local time scale $(dU^+/dy^+)^{-1}$, then, from principle 2 above, $(\Delta\omega^+)(dU^+dy^+)^{-1}$ must be proportional to $y^+\Delta\omega^+$; for similarity to be valid, this must be a function of $k_x^+y^+$ and $k_z^+y^+$ or, alternatively, k^+y^+ and α for a three-dimensional spectral function $P(k_x^+, k_z^+, \omega^+)$. That is, we must have

$$y^+\Delta\omega^+ = f(k_x^+y^+,\ k_z^+y^+) = f(k^+y^+, \alpha) \tag{13}$$

Substituting Eq. (12) into Eq. (13) and using Eq. (9), we get

$$C_x^+ - U^+ = g(k^+y^+, \alpha) \tag{14}$$

Equation (14) indicates that, for similarity to be valid, the term $[C_x^+ - U^+]$ for a constant wave angle α must be a function of k^+y^+ only. The convection velocity data obtained from the ridge lines of the power spectral density contours in Figs. 5 and 6 are plotted as $[C_x^+ - U^+]$ against k^+y^+ for various α as shown in Fig. 9. There is some scatter in the data, especially for small α, and the degree of scatter reduces as α increases. This trend of data scatter is a result of probe interference effects in the correlation measurements as described previously. For a given ω^+, convection velocity data are more affected by probe interference effects at large k^+ (that is, low α) than at small k^+ (large α). As seen from Fig. 9, for a given α the data for $y^+ = 70$ and 200 have approximately the same slope, and with a small shift in $[C_x^+ - U^+]$ they will collapse very well. In fact, to effect such a collapse for the worst case of $\alpha = 15$ deg requires only a shift of less than 0.6 in $[C_x^+ - U^+]$. This represents a total combined error of less than 3% in the calculation of the convection velocity from the power spectral density contours for $y^+ = 70$ and 200. Hence, within the limits of the conditions under which these data were obtained, the results in Fig. 9 tend to indicate that $[C_x^+ - U^+]$

is independent of y^+, lending support to the similarity hypothesis. The convection velocity results for $y^+ = 70$ and 200 at large wave angles such as $\alpha = 50$ deg agree with each other very well and are almost independent of k^+y^+, whereas, for small wave angles, they are a function of k^+y^+.

According to the geometrically similar wave model of Morrison and Kronauer,[10] the wave convection velocity C_x^+ matches the mean fluid velocity U^+ at a certain y^+, as given by Eq. (11). Rearranging Eq. (11) in the form similar to Eq. (14), we obtain

$$C_x^+(k^+y^+) - U^+(y_0^+) = 2.5\ \ell n\ (k^+y_0^+/k^+y^+) \qquad (15)$$

Equation (15) is a subset of Eq. (14) and is plotted in Fig. 9 for $k^+y_0^+ = 0.6$ for comparison with the present data. The model of Morrison and Kronauer[10] agrees very well with the data for small wave angles such as $\alpha = 10$ deg, but is not adequate to describe the data for large wave angles.

Spectral Sheet Thickness

The spectral sheet thickness $\Delta\omega^+$ can be obtained by measuring the full width between the half-power points in the (k_x^+,k_z^+) plot of the spectral function $P(k_x^+,k_z^+,\omega^+)$ in the k_x^+ direction, the half-width being Δk_x^+. Assuming that the spectral sheet is thin and very closely aligned with the locus $\omega^+ = k_x^+U^+$, we can deduce $\Delta\omega^+$ from the following relationship:

$$\Delta\omega^+ = \Delta k_x^+(\omega^+/k_x^+) \simeq U^+(y_0^+)\Delta k_x^+ \qquad (16)$$

By the same arguments used in deducing Eq. (13), $y_0^+\Delta\omega^+$ must be a function of k^+y^+ and α only, that is

$$y_0^+\Delta\omega^+ = h(k^+y^+,\alpha) \qquad (17)$$

The $y_0^+\Delta\omega^+$ data extracted using Eq. (16) from the spectral functions in Figs. 5 and 6 are plotted against k^+y^+ for three wave angles α in Fig. 10. For each α, although there is some scatter, the data for $y^+ = 70$ and 200 collapse onto a straight line in the logarithmic plot. Regression analysis indicates that, for all three wave angles, the lines of best fit as shown in Fig. 10 each gives a correlation coefficient 0.98 or better. In particular, the lines can be described by

$$2(y_0^+\Delta\omega^+) = C(\alpha)k^+y^+ \qquad (18)$$

where $C(\alpha) = 0.785 + 5.931\ \sin\alpha$, and α is measured in degrees for 20 deg $< \alpha <$ 50 deg. The variable $y_0^+\Delta\omega^+$ can also be regarded as a measure of the dissipation, which, according to Eqs. (18), is proportional to $\sin\alpha$, as is the component of the mean velocity profile in the $\hat{z}$ direction, that is, in the plane of the $\hat{w}$ waves. The waves span a range of α from 5 to 85 deg, so that the dissipation at large α ($\hat{w}$ waves) is almost 3.5 times that of the $\hat{u}$ waves, which propagate at small angles of approximately 10 deg.

Spectral Peaks

The typical size of a wave for a given wave angle can be characterized by the spectral peak. According to the similarity hypothesis, the locus of the spectral peaks should be independent of the absolute distance y^+ from the wall and is only dependent on $k_x^+y_0^+$ and $k_z^+y_0^+$. Consequently, the locations of spectral peaks in Fig. 7 have been replotted in Fig. 11 in $(k_x^+y_0^+,k_z^+y_0^+)$ space, and, as shown, they all collapse onto a straight line, supporting the similarity hypothesis. The line of best fit, yielding a correlation coefficient of 0.990, is given by

$$k_z^+y_0^+ = 0.51 + 1.21\ k_x^+y_0 \qquad (19)$$

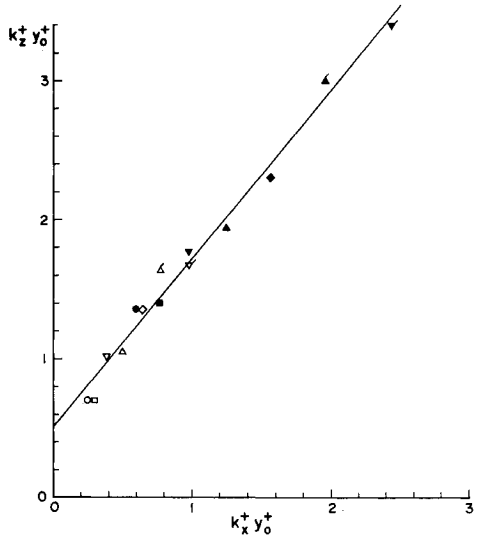

Fig. 11 Locus of spectral peaks in $(k_x^+y_0^+,k_z^+y_0^+)$ space: $y^+ = 70$, ○ $\omega^+ = 0.0536$, □ $\omega^+ = 0.0672$, ▽ $\omega^+ = 0.085$, △ $\omega^+ = 0.107$, ◇ $\omega^+ = 0.1347$, △ $\omega^+ = 0.17$, ▽ $\omega^+ = 0.2142$; $y^+ = 200$, ● $\omega^+ = 0.0536$, ■ $\omega^+ = 0.0672$, ▼ $\omega^+ = 0.085$, ▲ $\omega^+ = 0.107$, ◆ $\omega^+ = 0.1347$, ▲ $\omega^+ = 0.17$, ▼ $\omega^+ = 0.2142$.

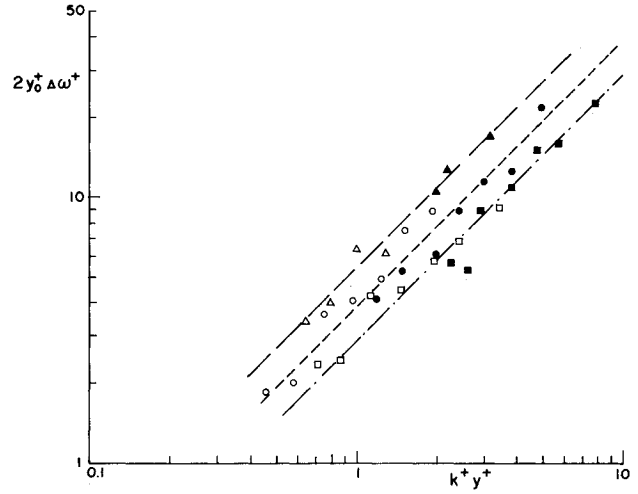

Fig. 10 Variation of $2y_0^+\ \Delta\ \omega^+$ with k^+y^+ for various α (symbols as in Fig. 9).

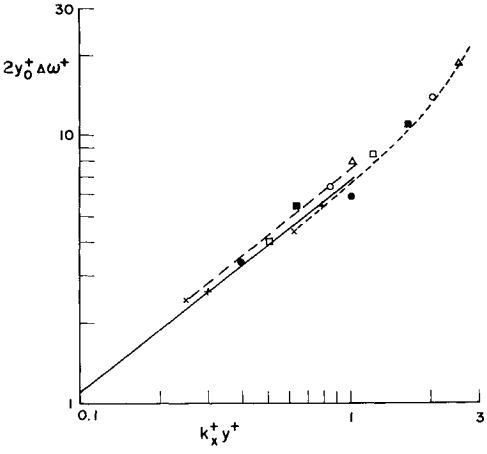

Fig. 12 Variation of $2y_0^+\ \Delta\ \omega^+$ [determined from $P(k_x^+,\omega^+)$] with $k_x^+y^+$ (symbols as in Fig. 7): —— Morrison and Kronauer data,[10] -- $y^+ = 70$, ---- $y^+ = 200$.

The range of $k_z^+ y_0^+$ is from 0.3 to 3.3, with the power concentrated at wave angles 10 to 35 deg, respectively.

Two-Dimensional Spectral Functions

In principle, similarity should apply equally well to the two-dimensional spectral function $P(k_x^+, \omega^+)$ as obtained by Morrison and Kronauer[10] and the three-dimensional spectral function $P(k_x^+, k_z^+, \omega^+)$ as obtained here, provided that spectral truncation effects due to minimum and maximum k^+ are not important and that Reynolds number effects are not significant if data for different Reynolds numbers are compared. To enable a comparison with the data of Morrison and Kronauer,[10] the three-dimensional spectral function data $P(k_x^+, k_z^+, \omega^+)$ obtained here are integrated over k_z^+ to give the two-dimensional spectral function $P(k_x^+, \omega^+)$ from which $y_0^+ \Delta\omega^+$ is extracted and plotted for $y^+ = 70$ and 200 against $k_x^+ y^+$ in Fig. 12. The agreement with the data of Morrison and Kronauer,[10] which only extend up to $k_x^+ y^+ = 1$, is excellent.

VII. Wave-Model Interpretation of the Data

As shown in Eq. (2), Morrison and Kronauer[10] deduced the intensity function $f(k^+ y^+)$, which peaks at a $k^+ y^+$ of 0.6 for waves of small α, and postulated that at larger distances from the wall the $\hat{w}$ component would predominate, so that the peak in the intensity function for these waves would occur at $k^+ y^+ = 2.4$. Near the wall, the apparent large-scale λ_x^+ wave is produced by measurement in a plane almost at right angles to the propagation direction k_z^+. The sublayer data reported by Morrison et al.[8] showed a λ_z^+ spacing of 135 and a λ_x^+ spacing of 630, giving an angle of propagation α of 12 deg, a $C_x^+ = 8.0$ with a critical layer height of $y_0^+ \simeq 9.0$. The data of Bullock et al.[9] confirm that the u component, especially at lower frequencies, correlates across the entire boundary layer and the magnitude of the correlation coefficient scales on $\omega^+ y^+$ related to $k_x^+ y^+$ through C_x^+, which has a narrow range. They also measured the phase advance of particular waves plotted at fixed values of $\omega^+ y^+$ and demonstrated a relationship of phase with $\omega^+ y^+$ which was linear over approximately 1.5 decades. They conclusively showed that the turbulence in the wall region lagged the outer layer, with the disturbances of a fixed geometry propagating toward the wall. At a value corresponding to $k_x^+ y^+ = 4$, there was a marked increase in phase, especially for the small-scale components, indicating a phase jump that could be associated with the critical height of the $\hat{w}$ components. The new data of Fig. 7 show that, for a specific wave size k^+, the angle of the wave increases as the measurement point y_0^+ increases. Thus, the results of Morrison and Kronauer,[10] Morrison et al.,[8] Bullock et al.,[9] and this recent work have produced quantitative measurements that substantiate not only the similarity hypothesis, postulated and accepted by many workers, for example, Perry and Abell,[11] but also the more interesting hypothesis of the wave model.

A physical interpretation of the method of generation of the wave-like phenomenon might be the following. In the presence of the high shear, the high-velocity fluid tends to roll over the lower-velocity fluid near the wall, producing an eddy whose size is characterized by the geometry of the flow. The eddy that produces wave-like components at high angle to the flow direction is twisted as it progresses downstream. The reorientation of the eddy is produced by the lower sections of the circulation moving into the high shear of the buffer layer, which not only produces large $\hat{u}$ components but also reduces the angle α to the flow. At large y^+, there is not as much $\hat{u}$ generated by the shear; therefore, the wave components are produced predominantly by $\hat{w}$, which is reflected in the measurement of the u component of velocity. Figure 13 of the data of Bullock et al.[9] shows the cross-power density spectrum between energy transfer in u at different y_1 and y_2 locations and demonstrates that the majority of the transfer of power occurs at relatively low frequency, for example, 0.004 in ω^+ for $y^+ = 700$ to 100. These data were also obtained with $u_\tau = 0.61$ m/s. It could be expected from the trends in Fig. 7 that the predominant α at $y^+ = 700$ would be approximately 60 deg. In this situation, the range in k_z^+ would be very much restricted. Thus, the coordination in y is much enhanced, and the phenomenon appearing would be more wave-like as the measurement station moves out, detecting more of the $\hat{w}$ waves that are likely to be centered with maximum intensity at $k^+ y^+ = 2.4$. Since all physical systems must be continuous functions, it is most likely that, if data were recorded at $y^+ = 700$, then $k_z^+ y^+$ of the similarity hypothesis would move nearer to the peak expected of $k^+ y^+ = 2.4$.

VIII. Conclusions

Extensive two-dimensional filtered correlation measurements in the longitudinal velocity fluctuation $R(x^+, z^+ | \omega^+)$ at two fixed distances from the wall $y^+ = 70$ and 200 for a friction velocity of 0.61 m/s have been described. The power spectral density function $P(k_x^+, k_z^+, \omega^+)$ obtained from the Fourier transform of the cross correlation $R(x^+, z^+ | \omega^+)$ has been presented as contour plots in wave number space, which indicates the following:

1) At $y^+ = 70$, the power is distributed over a range of wave angle 6 deg $< \alpha <$ 74 deg and a range of wave sizes $0.004 < k^+ < 0.07$.

2) At $y^+ = 200$, the power is distributed over a range of wave angle 9 deg $< \alpha <$ 81 deg and a range of wave sizes $0.003 < k^+ < 0.0611$.

The convection velocity results determined from the spectral density function contours explain the controversial data of McConachie.[15] The data for convection velocity, spectral sheet thickness, and spectral peaks at two different y^+ substantially verify the similarity hypothesis. However, the geometrically similar wave model of Morrison and Kronauer[10] is valid only for small wave angles.

Acknowledgments

The experiment described here was conducted while the first author was a Postdoctoral Fellow at the University of Queensland. The authors would like to acknowledge the contribution of R. Gammie, who designed the traversing mechanism, B. Daniel, who designed the digital controller for the traversing mechanism, and J. Brennan for his expert skills in repairing damaged hot wires endlessly.

References

[1]Runstadler, P. W., Kline, S. J., and Reynolds, W. C., "An Experimental Investigation of the Flow Structure of the Turbulent Boundary Layer," Stanford Univ., Stanford, CA, Dept. of Mechanical Engineering, Rept. MD-8, 1963.

[2]Kim, H. T., Kline, S. J., and Reynolds, W. C., "The Production of Turbulence near a Smooth Wall in a Turbulent Boundary Layer," *Journal of Fluid Mechanics,* Vol. 50, Pt. 1, Nov. 1971, p. 133.

[3]Corino, E. R. and Brodkey, R. S., "A Visual Investigation of the Wall Region in Turbulent Flow," *Journal of Fluid Mechanics,* Vol. 37, Pt. 1, June 1969, p. 1.

[4]Kline, S. J., Reynolds, W. C., Schrabb, F. A., and Runstadler, P. W., "The Structure of Turbulent Boundary Layers," *Journal of Fluid Mechanics,* Vol. 30, Pt. 4, Dec. 1967, p. 741.

[5]Laufer, J., "The Structure of Turbulence in Fully Developed Pipe Flow," NACA Rept. 1174, 1954.

[6]Tritton, D. J., "Some New Correlation Measurements in a Turbulent Boundary Layer," *Journal of Fluid Mechanics,* Vol. 28, Pt. 3, May 1967, p. 439.

[7]Fage, A. and Townend, H. C. H., "An Examination of Turbulent Flow with an Ultra-Microscope," *Proceedings of the Royal Society of London, Series A,* Vol. 135, 1932, p. 656.

[8]Morrison, W. R. B., Bullock, K. J., and Kronauer, R. E., "Experimental Evidence of Waves in the Sublayer," *Journal of Fluid Mechanics,* Vol. 47, Pt. 4, June 1971, p. 639.

[9]Bullock, K. J., Cooper, R. E., and Abernathy, F. H., "Structural Similarity in Radial Correlations and Spectra of Longitudinal Velocity Fluctuations in Pipe Flow," *Journal of Fluid Mechanics,* Vol. 88, 1978, p. 585.

[10]Morrison, W. R. B. and Kronauer, R. E., "Structural Similarity for Fully Developed Turbulence in Smooth Tubes," *Journal of Fluid Mechanics,* Vol. 39, Pt. 1, Oct. 1969, p. 117.

[11]Perry, A. E. and Abell, C. J., "Scaling Laws for Pipe-flow Turbulence," *Journal of Fluid Mechanics,* Vol. 67, Pt. 2, Jan. 1975, p. 257.

[12]Bull, M. K., "Wall Pressure Fluctuations Associated with Subsonic Turbulent Boundary Layer Flow," *Journal of Fluid Mechanics,* Vol. 28, Pt. 4, June 1967, p. 719.

[13]Elliot, J. A., "Microscale Pressure Fluctuations Measured within the Lower Atmospheric Boundary Layer," *Journal of Fluid Mechanics,* Vol. 53, Pt. 2, May 1972, p. 351.

[14]McConachie, P. J. and Bullock, K. J., "Measurement of Turbulence Close to a Wall with Temperature Wake Sensing Probe," *Journal of Physics E: Scientific Instruments,* Vol. 9, Oct. 1976, p. 862.

[15]McConachie, P. J., "The Distribution of Convection Velocities in Turbulent Pipe Flow," *Journal of Fluid Mechanics,* Vol. 103, Feb. 1981, p. 65.

[16]Comte-Bellot, G., Strohl, A., and Alcarex, E., "On Aerodynamic Disturbances Caused by Single Hot Wire Probes," *Journal of Applied Mechanics,* Vol. 38, 1971, p. 767.

Recommended Reading from the AIAA Progress in Astronautics and Aeronautics Series . . .

Thrust and Drag: Its Prediction and Verification

Eugene E. Covert, C. R. James, W. M. Kimzey, G. K. Richey, and E. C. Rooney, editors

Gives an authoritative, detailed review of the state-of-the-art of prediction and verification of the thrust and drag of aircraft in flight. It treats determination of the difference between installed thrust and drag of an aircraft and how it is complicated by interaction between inlet airflow and flow over the boattail and other aerodynamic surfaces. Following a brief historical introduction, chapters explore the need for a bookkeeping system, describe such a system, and demonstrate how aerodynamic interference can be explained. Subsequent chapters illustrate calculations of thrust, external drag, and throttle-induced drag, and estimation of error and its propagation. A commanding overview of a central problem in modern aircraft design.

TO ORDER: Write AIAA Order Department, 370 L'Enfant Promenade, S.W., Washington, DC 20024

Please include postage and handling fee of $4.50 with all orders. California and D.C. residents must add 6% sales tax. All orders under $50.00 must be prepaid. All foreign orders must be prepaid. Please allow 4-6 weeks for delivery. Prices are subject to change without notice.

1985 346 pp., illus. Hardback
ISBN 0-930403-00-2
AIAA Members $49.95
Nonmembers $69.95
Order Number V-98